

Reducing Two-Way Ranging Variance by Signal-Timing Optimization

Mohammed Ayman Shalaby, Student Member, IEEE
McGill University, Montreal, QC, Canada

Charles Champagne Cossette, Student Member, IEEE
McGill University, Montreal, QC, Canada

James Richard Forbes, Member, IEEE
McGill University, Montreal, QC, Canada

Jerome Le Ny, Senior Member, IEEE
Polytechnique Montreal, Montreal, QC, Canada

Abstract— Time-of-flight-based ranging among transceivers with different clocks requires protocols that accommodate varying rates of the clocks. Double-sided two-way ranging (DS-TWR) is widely adopted as a standard protocol due to its accuracy; however, the precision of DS-TWR has not been clearly addressed. In this paper, an analytical model of the variance of DS-TWR is derived as a function of the user-programmed response delays, which is then compared to the *Cramer-Rao Lower Bound* (CRLB). This is then used to formulate an optimization problem over the response delays in order to maximize the information gained from range measurements. The derived analytical variance model and optimized protocol are validated experimentally with 2 ranging UWB transceivers, where 29 million range measurements are collected.

Index Terms— ultra-wideband, ranging, Cramer-Rao lower bound, localization.

I. Introduction

A common requirement for real-time localization systems (RTLS) is a source of distance or *range* measurements between different bodies, which motivated the adoption of the IEEE 802.15.4a standard [1] for radio-frequency systems. Range measurements are obtained by measuring the time-of-flight (ToF) of signals between two transceivers, which requires accurate timestamping of transmission and reception of signals at both

This work was supported by the NSERC Alliance Grant program, the NSERC Discovery Grant program, the CFI JELF program, and FRQNT Award 2018-PR-253646. (Corresponding author: M. A. Shalaby).

Mohammed A. Shalaby, Charles C. Cossette, and James R. Forbes are with the Mechanical Engineering Department, McGill University, Montreal, QC H3A 0C3, Canada (e-mails: mohammed.shalaby@mail.mcgill.ca, charles.cossette@mail.mcgill.ca, james.richard.forbes@mcgill.ca). Jerome Le Ny is with the Electrical Engineering Department, Polytechnique Montreal, Montreal, QC H3T 1J4, Canada (e-mail: jerome.le-ny@polymtl.ca).

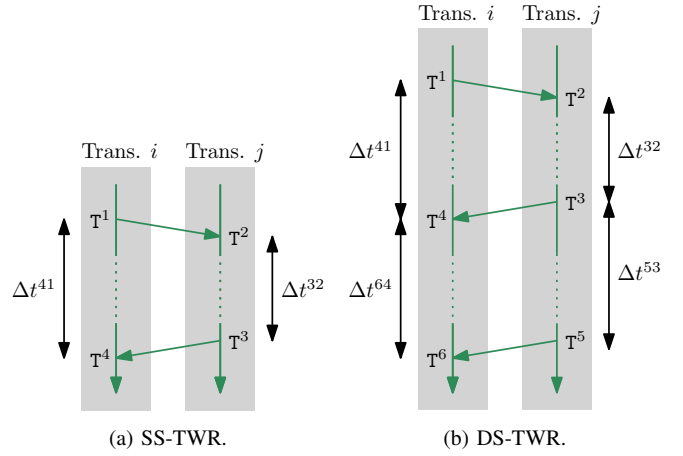


Fig. 1: Timeline schematics for two transceivers i and j showing the different TWR ranging protocols, where T^ℓ denotes the ℓ^{th} timestamp for a TWR instance and $\Delta t^{k\ell} \triangleq T^k - T^\ell$.

transceivers. However, this is not straightforward due to the transceivers' clocks running at different rates, thus introducing a time-varying offset between the clocks [2], [3], [4]. The rate of change of this clock offset is hereinafter referred to as the *clock skew*.

The clock offsets and skews between different transceivers introduce biases in the range measurements [5], [6], [7], which are addressed by the ranging protocols presented in the IEEE 802.15.4z standard [8]. A commonly used protocol is *two-way ranging* (TWR), which relies on averaging out two ToF measurements in order to negate the effect of the clock offset. This is widely adopted in ultra-wideband (UWB)-based ranging [7], [9], [10], and is also used in underwater applications utilizing acoustic position systems [11], distance measuring equipment (DME) in aviation navigation [12], and other radio systems such as Zigbee [13].

This paper focuses on two variants of the TWR protocol, particularly the single-sided TWR (SS-TWR) and the double-sided TWR (DS-TWR) protocols presented in [7], both shown in Figure 1. Despite requiring an additional message transmission, the main motivation behind DS-TWR as compared to SS-TWR is to correct the clock-skew-dependent bias, which improves the accuracy of the measurements [6], [7]. DS-TWR can also be used in the correction of other sources of error, such as the warm-up error [14]. Nonetheless, the *precision* of DS-TWR measurements as compared to SS-TWR measurements is a less commonly-addressed topic, where precision is typically measured by the variance of the range measurements. The variance of TWR measurements has been derived analytically as an approximate function of the true range [15], [16], the low-level features of the signal such as the pulse shape [17], the surrounding environment [15], or experimentally for some fixed timing intervals [18].

The main focus of this paper is to extend the comparison between SS-TWR and DS-TWR measurements to include the variance as a function of the timing delays

in between message transmissions as shown in Figure 1, which allows optimizing signal timing in DS-TWR to improve precision. Currently, the length of timing delays is arbitrarily chosen; for example, the default DS-TWR code for the commonly-used DW1000 UWB modules [19] appears to include arbitrarily-chosen timing delays without any justification. This paper therefore presents an easily-implementable approach to setting these delays to improve the precision of the range measurements, which in the case of the DW1000 modules is as simple as changing one number in the default code.

The contributions of this paper are as follows.

- Deriving an analytical model of the variance of SS-TWR and DS-TWR that is a function of the timing of message transmissions.
- Comparing the derived DS-TWR analytical variance to the *Cramer-Rao Lower Bound* (CRLB).
- Formulating an optimization problem for DS-TWR that is a function of the signal timings to maximize the information collected in one unit of time.
- Analyzing the effect of relative motion during ranging for DS-TWR.
- Validating experimentally the analytical model and the optimization procedure using static UWB transceivers.

The remainder of this paper is organized as follows. The analytical model of the variance and CRLB of TWR measurements is derived in Section II, and the timing-optimization problem is formulated in Section III. Experimental validation is then shown in Section IV.

A. Notation

The i^{th} time instance in a TWR transaction is denoted $T^i \in \mathbb{R}$ as shown in Figure 1, and T_j^i denotes the i^{th} time instance as timestamped by Transceiver j . The length of time between two time instances ℓ and k is denoted $\Delta t^{k\ell} \triangleq T^k - T^\ell$. These can also be resolved in a Transceiver's clock, such as $\Delta t_j^{k\ell} = T_j^k - T_j^\ell$. The ToF between Transceivers i and j is denoted t_f , and an estimate of the ToF is denoted \hat{t}_f . The time-varying *clock offset* $\tau_i(t)$ of Transceiver i is defined as $t_i(t) = t + \tau_i(t)$, where $t_i(t)$ is the time t resolved in Transceiver i 's clock. The *clock skew* of Transceiver i is denoted γ_i and is defined as $\tau_i(t + \Delta t) = \tau_i(t) + \gamma_i(t)\Delta t$.

II. TWR Variance

A. Modelling the Timestamps

The measurement models for the timestamps recorded by Transceivers i and j in Figure 1 are first presented under the assumption that all transceivers are static. The noisy timestamps recorded by Transceiver i in Figure 1a are modelled as

$$T_i^1 = T^1 + \tau_i(T^1) + \eta^1, \quad (1)$$

$$T_i^4 = T^1 + 2t_f + \Delta t^{32} + \tau_i(T^4) + \eta^4, \quad (2)$$

where η^ℓ is random noise on the ℓ^{th} measurement. All random noise variables on timestamps are assumed to be mutually independent, zero-mean, and with the same variance R .

Similarly, the noisy timestamps recorded by Transceiver j in Figure 1a are modelled as

$$T_j^2 = T^1 + t_f + \tau_j(T^2) + \eta^2, \quad (3)$$

$$T_j^3 = T^1 + t_f + \Delta t^{32} + \tau_j(T^3) + \eta^3, \quad (4)$$

while the additional timestamps when performing DS-TWR as in Figure 1b are modelled as

$$T_j^5 = T^1 + t_f + \Delta t^{32} + \Delta t^{53} + \tau_j(T^5) + \eta^5, \quad (5)$$

$$T_i^6 = T^1 + 2t_f + \Delta t^{32} + \Delta t^{53} + \tau_i(T^6) + \eta^6. \quad (6)$$

Throughout this paper, the approximation $\gamma_i \Delta t^{41} \approx \gamma_i \Delta t^{32}$ is made since clock skews are small and Δt^{32} is in the order of a few hundred microseconds, which is much greater than $2t_f$ for short range systems. Additionally, it is assumed that clock skews are constant during a ranging transaction, which is a common assumption in localization applications due to the clocks' slow dynamics [3], [6].

B. Deriving SS-TWR Variance

A SS-TWR ToF estimate \hat{t}_f^{ss} of the true ToF t_f can be computed from (1)-(4) as

$$\begin{aligned} \hat{t}_f^{\text{ss}} &= \frac{1}{2}(\Delta t_i^{41} - \Delta t_j^{32}) \\ &= \frac{1}{2}(2t_f + \Delta t^{32} + \gamma_i \Delta t^{41} + \eta^{41} - (1 + \gamma_j)\Delta t^{32} - \eta^{32}) \\ &\approx t_f + \frac{1}{2}\gamma_{ij}\Delta t^{32} + \frac{1}{2}(\eta^{41} - \eta^{32}), \end{aligned}$$

where $\gamma_{ij} \triangleq \gamma_i - \gamma_j$, $\eta^{k\ell} \triangleq \eta^k - \eta^\ell$, and $\gamma_i \Delta t^{41} \approx \gamma_i \Delta t^{32}$. Defining the SS-TWR ToF error as $e^{\text{ss}} \triangleq \hat{t}_f^{\text{ss}} - t_f$, the expected value of the error is

$$\mathbb{E}[e^{\text{ss}}] = \frac{1}{2}\gamma_{ij}\Delta t^{32}, \quad (7)$$

which means that \hat{t}_f^{ss} is in fact a biased measurement of t_f . Meanwhile, the covariance on the measurement is

$$\mathbb{E}[(e^{\text{ss}} - \mathbb{E}[e^{\text{ss}}])^2] = R. \quad (8)$$

C. DS-TWR Variance

The main motive behind using DS-TWR protocols rather than SS-TWR protocols is to correct the clock-skew-dependent bias in (7). As shown in [7, Eq. (6)], the DS-TWR ToF estimate from (1)-(6) can be modelled as

$$\hat{t}_f^{\text{ds}} = \frac{1}{2} \left(\Delta t_i^{41} - \frac{\Delta t_i^{64}}{\Delta t_j^{53}} \Delta t_j^{32} \right) \quad (9)$$

$$\approx t_f + \frac{1}{2} \left(\frac{\Delta t_j^{32}}{\Delta t_j^{53}} (\eta^{53} - \eta^{64}) + \eta^{41} - \eta^{32} \right), \quad (10)$$

where the approximations $\gamma_i t_f \approx 0$ and $\gamma_i \eta \approx 0$ are used since the clock skew, time-of-flight, and timestamping

noise are all small. Defining the DS-TWR ToF error as $e^{\text{ds}} \triangleq \hat{t}_f^{\text{ds}} - t_f$, the expected value of the error is

$$\mathbb{E}[e^{\text{ds}}] = 0,$$

meaning that unlike \hat{t}_f^{ss} , the estimate \hat{t}_f^{ds} is unbiased.

Having addressed the accuracy of the measurements for SS-TWR and DS-TWR, it might appear that DS-TWR should always be used. However, the choice of ranging protocol should also depend on the precision of the measurements. By manipulating (10), the covariance of \hat{t}_f^{ds} can be found to be of the form

$$\mathbb{E}[(e^{\text{ds}} - \mathbb{E}[e^{\text{ds}}])^2] = R \left(1 + \frac{\Delta t^{32}}{\Delta t^{53}} + \left(\frac{\Delta t^{32}}{\Delta t^{53}} \right)^2 \right). \quad (11)$$

Therefore, the variance of DS-TWR measurements is greater than SS-TWR measurements, and approaches the variance of SS-TWR as $\Delta t^{32} \rightarrow 0$ and/or $\Delta t^{53} \rightarrow \infty$. The $\Delta t^{32} \rightarrow 0$ condition is due to the effect of the length of Δt^{32} on the bias, and the $\Delta t^{53} \rightarrow \infty$ condition is due to the fact that the ratio $\frac{\Delta t^{64}}{\Delta t^{53}}$ is being used to obtain a clock-skew measurement, and the longer the Δt^{53} interval is the greater the signal-to-timestamping-noise ratio.

D. Cramer-Rao Bound of DS-TWR

Given that now an analytical model is available of the variance of the range estimate provided by the DS-TWR protocol (9), the variance of the estimator can be compared to the CRLB [20, Chapter 3].

When two transceivers are ranging with one another, time instances in global time and offsets of individual clocks remain unknown, and only the time instances in a transceiver's clocks and relative offset between the two Transceivers can be estimated. Therefore, the unknown quantities to be estimated from (1)-(6) can be summarized in a state vector

$$\mathbf{x} = [t_f \quad \mathcal{T} \quad \tau_{ij} \quad \gamma_{ij} \quad \Delta t_j^{32} \quad \Delta t_j^{53}]^T,$$

where $\mathcal{T} = \mathbf{T}^1 + \tau_i(\mathbf{T}^1)$ and $\tau_{ij} \triangleq \tau_i(\mathbf{T}^1) - \tau_j(\mathbf{T}^1)$. Additionally, under the assumption that $\frac{\gamma_{ij}}{1+\gamma_j} \approx \gamma_{ij}$ since $\gamma_j \ll 1$, it can be shown that

$$\begin{aligned} \Delta t_i^{32} &\approx (1 + \gamma_{ij})\Delta t_j^{32}, \\ \Delta t_i^{53} &\approx (1 + \gamma_{ij})\Delta t_j^{53}. \end{aligned}$$

Therefore, the timestamp measurements (1)-(6) can be written as

$$\begin{aligned} \mathbf{T}_i^1(\mathbf{x}) &= \mathcal{T} + \eta^1, \\ \mathbf{T}_j^2(\mathbf{x}) &= \mathcal{T} + t_f - \tau_{ij} + \eta^2, \\ \mathbf{T}_j^3(\mathbf{x}) &\approx \mathcal{T} + t_f - \tau_{ij} + \Delta t_j^{32} + \eta^3, \\ \mathbf{T}_i^4(\mathbf{x}) &\approx \mathcal{T} + 2t_f + (1 + \gamma_{ij})\Delta t_j^{32} + \eta^4, \\ \mathbf{T}_j^5(\mathbf{x}) &\approx \mathcal{T} + t_f - \tau_{ij} + \Delta t_j^{32} + \Delta t_j^{53} + \eta^5, \\ \mathbf{T}_i^6(\mathbf{x}) &\approx \mathcal{T} + 2t_f + (1 + \gamma_{ij})(\Delta t_j^{32} + \Delta t_j^{53}) + \eta^6, \end{aligned}$$

where the approximation $\gamma_i t_f \approx 0$ has been used. The measurement vector can then be written as

$$\mathbf{y}(\mathbf{x}) = [\mathbf{T}_i^1 \quad \mathbf{T}_j^2 \quad \mathbf{T}_j^3 \quad \mathbf{T}_i^4 \quad \mathbf{T}_j^5 \quad \mathbf{T}_i^6]^T,$$

which is a nonlinear function of the states \mathbf{x} . Therefore, the measurement Jacobian can be computed as

$$\mathbf{C} = \left. \frac{\partial \mathbf{y}(\mathbf{x})}{\partial \mathbf{x}} \right|_{\bar{\mathbf{x}}} = \begin{bmatrix} 0 & 1 & 0 & 0 & 0 & 0 \\ 1 & 1 & -1 & 0 & 0 & 0 \\ 1 & 1 & -1 & 0 & 1 & 0 \\ 2 & 1 & 0 & \Delta \bar{t}_j^{32} & 1 + \bar{\gamma}_{ij} & 0 \\ 1 & 1 & -1 & 0 & 1 & 1 \\ 2 & 1 & 0 & \Delta \bar{t}_j^{32} + \Delta \bar{t}_j^{53} & 1 + \bar{\gamma}_{ij} & 1 + \bar{\gamma}_{ij} \end{bmatrix},$$

where overbars denote the linearization point. Additionally, define a measurement vector covariance $\mathbf{R} \triangleq R\mathbf{I}_6$, where \mathbf{I}_6 is the 6×6 identity matrix.

The CRLB states that the covariance of any unbiased estimate $\hat{\mathbf{x}}$ of \mathbf{x} , given the measurements $\mathbf{y}(\mathbf{x})$ and an additive-Gaussian assumption on the measurement noise, is bounded by [20, Appendix 3C]

$$\mathbb{E}[(\mathbf{x} - \hat{\mathbf{x}})(\mathbf{x} - \hat{\mathbf{x}})^T] \geq (\mathbf{C}^T \mathbf{R}^{-1} \mathbf{C})^{-1}.$$

The minimum variance of the ToF estimate for the given timestamps can then be found by extracting the first component of $(\mathbf{C}^T \mathbf{R}^{-1} \mathbf{C})^{-1}$, which can be found to be

$$R \frac{(\bar{\gamma}_{ij}^2 + 2\bar{\gamma}_{ij} + 2)((\Delta \bar{t}_j^{32})^2 + \Delta \bar{t}_j^{32} \Delta \bar{t}_j^{53} + (\Delta \bar{t}_j^{53})^2)}{2(\Delta \bar{t}_j^{53})^2}.$$

Given that $\bar{\gamma}_{ij}^2 + 2\bar{\gamma}_{ij} \ll 2$, this can be simplified to give exactly (11), thus showing that under the aforementioned approximations the DS-TWR estimator is indeed minimum-variance unbiased estimator.

III. DS-TWR Timing Optimization

The *timing delays* Δt^{32} and Δt^{53} affect the variance of the range measurements, the rate of the measurements, and the ranging error due to relative motion between the transceivers. In Section A, the choice of delays is motivated as a function of the variance and rate of the measurements while assuming no relative motion between the transceivers. This assumption is then validated in Section B for the DS-TWR protocol, showing that motion can indeed be neglected when choosing the timing delays.

A. Finding Optimal Timing Delays

Given (11), minimizing Δt^{32} within the limitations of the system is an obvious choice to reduce the measurement variance. However, it is less clear what the right choice for Δt^{53} is, as increasing this second-response delay reduces measurement variance but also reduces the rate of measurements. The choice of Δt^{53} is thus application-specific. Most commonly in estimation applications, the goal is to minimize the variance of the estimates, which is achieved by maximizing the *information* attained from measurements. Therefore, this section poses an information-maximizing (variance-minimizing) optimization problem.

The amount of information obtained in one unit of time is a function of the variance of the individual measurement and the number of measurements in that unit of time. As a result, the *optimal* delay is one that is long enough to reduce the variance of the individual measurement but short enough to ensure measurements are recorded at a sufficient rate.

The rate of the measurements is dependent on $\Delta t^{32} + \Delta t^{53}$ as well as any further processing required to retrieve the range measurements, such as reading the raw timestamps from the registers and computing the range measurement from the raw timestamps. The time taken for computational processing is defined as T , which is assumed to be constant for the same experimental set-up. Therefore, the time-length of one measurement is $T + \Delta t^{32} + \Delta t^{53}$ seconds long. The delay Δt^{32} is to be minimized as much as the hardware allows, and Δt^{53} is to be optimized as follows. In one second, a total of $\left[\frac{1}{T + \Delta t^{32} + \Delta t^{53}}\right]$ measurements occur, meaning that the variance of averaging out the ToF estimates is, assuming independence, given as

$$R_{\text{avg}}(\Delta t^{53}) \triangleq [T + \Delta t^{32} + \Delta t^{53}]R_{\text{meas}}(\Delta t^{53}), \quad (12)$$

where $R_{\text{meas}}(\Delta t^{53})$ is the variance of the individual measurement given by (11) for some constant Δt^{32} . R_{avg} is referred to hereinafter as the *averaged uncertainty*, and can be thought of as the inverse of accumulated *information* in one second. Finding the optimal delay Δt^{53*} is then found by solving

$$\Delta t^{53*} = \arg \min_{\Delta t^{53} \in \mathbb{R}} R_{\text{avg}}(\Delta t^{53}). \quad (13)$$

The derivative of (12) with respect to Δt^{53} is

$$\begin{aligned} \frac{dR_{\text{avg}}}{d\Delta t^{53}} &= R - (T + \Delta t^{32}) \frac{\Delta t^{32}}{(\Delta t^{53})^2} R \\ &\quad - 2(T + \Delta t^{32}) \frac{(\Delta t^{32})^2}{(\Delta t^{53})^3} R - \frac{(\Delta t^{32})^2}{(\Delta t^{53})^2} R, \end{aligned}$$

and equating to 0 yields the cubic polynomial

$$\begin{aligned} 0 &= (\Delta t^{53})^3 - \Delta t^{32}(T + 2\Delta t^{32})\Delta t^{53} \\ &\quad - 2(\Delta t^{32})^2(T + \Delta t^{32}). \end{aligned} \quad (14)$$

This is a ‘‘depressed cubic equation’’ that can be solved analytically using Cardano’s method, but the analytical solution is omitted here for conciseness. Additionally, this can be solved programatically using standard libraries, such as Bullet’s `cubic_roots` function in C++ or NumPy’s `roots` function in Python.

The value for T and the minimum value of Δt^{32} can be determined experimentally and are both processor and application dependent. As an example where $T = 7.2$ ms and $\Delta t^{32} = 0.35$ ms, the optimal delay can be found analytically to be approximately 1.9 ms using (14). The averaged variance R_{avg} as a function of Δt^{53} for $T = 7.2$ ms at different values of Δt^{32} is shown in Figure 2. As expected from (11), the averaged variance R_{avg} explodes as Δt^{53} approaches 0 ms.

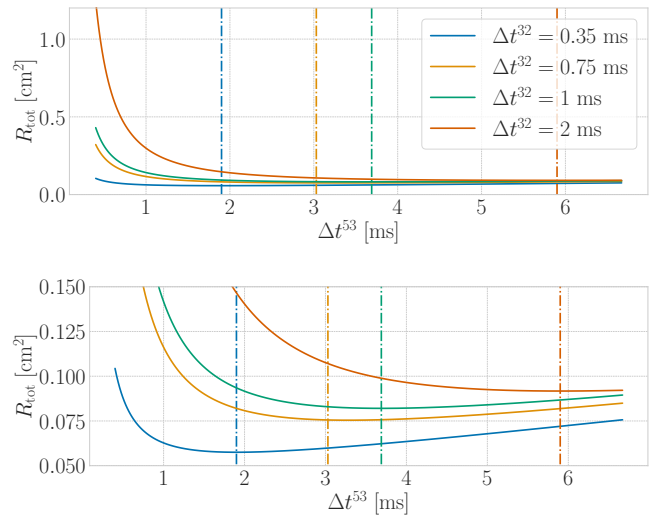


Fig. 2: The theoretical averaged variance R_{avg} as a function of the delay Δt^{53} for 4 different values of Δt^{32} . All curves use $T = 7.2$ ms, which is experimentally determined for the set-up used in Section IV. The vertical dotted lines correspond to the analytically-evaluated minimum of the colour-matched plotted curves. The bottom plot is a close-up view of the top plot. Note that R_{avg} is converted from units of $[\text{s}]^2$ to $[\text{cm}]^2$ by multiplying with c^2 $[\text{cm}^2/\text{s}^2]$, where c is the speed of light, in order to visualize the variance on the range measurements directly.

B. Relative Motion During Ranging

A constant distance throughout ranging is commonly assumed, but this assumption introduces larger errors for longer response delays. To address this, assume the less-restrictive case of no relative acceleration between the transceivers. In this case, the three ToF measurements shown in Figure 1b are of different distances, and are related by

$$t_f^2 = t_f^1 + \bar{v}\Delta t^{32}, \quad t_f^3 = t_f^2 + \bar{v}\Delta t^{53},$$

where t_f^i is the ToF of the i^{th} message, $\bar{v} = v/c$, v is the rate of change of the distance between transceivers, and c is the speed of light. Note that motion during the intervals Δt^{32} and Δt^{53} is addressed since the intervals are in the order of milliseconds. Meanwhile, ToF is in the order of nanoseconds for short range measurements, so motion in between time of transmission and reception is negligible.

The computed ToF measurement using the DS-TWR protocol in the absence of clock offsets, skews, and timestamping noise is then

$$\begin{aligned} \hat{t}_f^{\text{ds}} &= \frac{1}{2} \left(\Delta t^{41} - \frac{\Delta t^{64}}{\Delta t^{53}} \Delta t^{32} \right) \\ &= \frac{1}{2} \left(t_f^1 + \Delta t^{32} + t_f^2 - \frac{\Delta t^{53} + t_f^3 - t_f^2}{\Delta t^{53}} \Delta t^{32} \right) \\ &= \frac{1}{2} \left(2t_f^1 + (1 + \bar{v})\Delta t^{32} - \frac{(1 + \bar{v})\Delta t^{53}}{\Delta t^{53}} \Delta t^{32} \right) \\ &= t_f^1, \end{aligned}$$

meaning that the computed ToF corresponds to the distance between the transceivers at the beginning of ranging, and the error due to motion is independent from the delays Δt^{32} and Δt^{53} . Therefore, a particular feature of



Fig. 3: The experimental set-up. (Left) Custom-built circuit board, using the DWM1000 UWB transceiver. (Right) Two static tripods placed 1.5 metres apart, each holding a UWB transceiver.

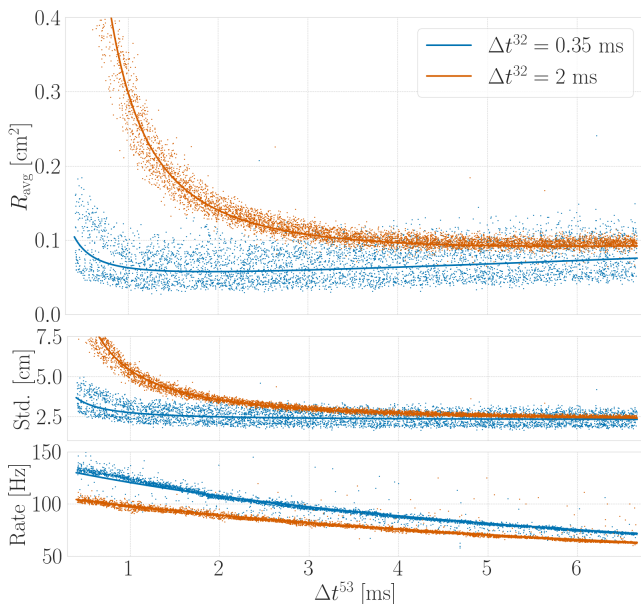


Fig. 4: The theoretical and experimental metrics as they vary with Δt^{53} . Each point corresponds to one trial of 2500 measurements, and the solid line is the theoretical curve based on the derived analytical models. The solid line matches the experimental readings. The plots show the variation of the averaged variance R_{avg} as given by (12), the standard deviation as given by the square root of (11), and the rate of the measurements as a function of Δt^{53} for two different values of Δt^{32} .

the DS-TWR protocol presented in [7] is that the timing optimization can be done without addressing errors due to motion. A similar analysis on the DS-TWR protocol proposed in [6] shows that the error in the ranging measurements due to motion is a complicated function of the velocity and the delays.

IV. Experimental Evaluation

To evaluate the effect of the second-response delay Δt^{53} on a real system, the following experiment is performed. Two custom-made circuit boards equipped with

DWM1000 UWB transceivers [19] are fixed to two static tripods as shown in Figure 3. They are both connected to a Dell XPS13 computer running Ubuntu Desktop 20.04. The second-response delay Δt^{53} is then sampled randomly many times, and for each trial 2500 measurements are collected to compute the average variance and rate for that specific value of Δt^{53} . The results for two different values of Δt^{32} are shown in Figure 4, where $T = 7.2$ ms is found experimentally to be the time required by the computer to process a range measurement. The experiment with $\Delta t^{32} = 0.35$ ms involves 5000 trials for a total of 12.5 million measurements, while the experiment with $\Delta t^{32} = 2$ ms involves 6600 trials for a total of 16.5 million measurements.

Given that this is a static experiment, R_{avg} essentially represents the variance in the measurement obtained by averaging out all recorded measurements over a span of one second. Crucially, both experiments presented here match the theoretical expectations quite well. As Δt^{53} increases, both the standard deviation and the rate of the measurements decrease, and the optimal Δt^{53} can then be found by finding the value that minimizes R_{avg} . The experimental minimum does match the theoretical minimum, thus motivating the presented analytical optimization problem (13). Lastly, as expected, the experiments with a longer Δt^{32} have an order of magnitude higher standard deviation in the measurements, and in both experiments the standard deviation decreases as Δt^{53} increases.

In addition to the DS-TWR experiment, a SS-TWR experiment is performed with 145 trials, for a total of 362500 measurements. Nothing varied in between trials, but the purpose of this experiment is to obtain the average standard deviation of SS-TWR experiments in order to evaluate whether the DS-TWR standard deviation does indeed converge to that of SS-TWR as $\Delta t^{53} \rightarrow \infty$ as suggested in Section II. The SS-TWR standard deviation is found to be about 2.8 cm, while the curves in Figure 4 converge to a standard deviation of approximately 2.5 cm. The slightly higher SS-TWR variance is due to the effect of clock skew, as the SS-TWR measurements drift over the 2500 range measurements of a single trial, which increases the computed standard deviation.

V. Conclusion

This paper extends the comparison of SS-TWR and DS-TWR to include precision by deriving an analytical model of the variance and the CRLB as a function of the signal timings of the ranging protocols. This consequently allows optimizing over the timing delays in order to minimize the variance of DS-TWR measurements, and an optimization problem is then formulated to maximize information by balancing the effect of reduced variance and reduced rate of measurements as timing delays increase. It is also shown that the effect of motion is independent of the timing delays in the utilized DS-TWR protocol. Lastly, the analytical variance model and optimization

procedure are evaluated on an experimental set-up with two static ranging UWB transceivers. Future work will address finding optimal delays when the ranging protocol is customizable beyond standard DS-TWR, or when new TWR instances can be initiated before others are done.

REFERENCES

- [1] IEEE Computer Society, *IEEE Standard for Low-Rate Wireless Networks. Amendment 1: Add Alternate PHYs (IEEE Std 802.15.4a)*, Number 2. 2018.
- [2] Alan Binsky, *Wireless Positioning Technologies and Applications*, Artech House, Inc., USA, 2007.
- [3] Zafer Sahinoglu, Sinan Gezici, and Ismail Güvenc, *Ultra-wideband Positioning Systems: Theoretical Limits, Ranging Algorithms, and Protocols*, Cambridge University Press, 2008.
- [4] Vaclav Navratil, Josef Krska, and Frantisek Vejrazka, “Concurrent Bidirectional TDoA Positioning in UWB Network with Free-Running Clocks,” *IEEE Trans. on Aerospace and Electronic Systems*, vol. 58, no. 5, pp. 4434–4450, 2022.
- [5] Myungkyun Kwak and Jongwha Chong, “A new double two-way ranging algorithm for ranging system,” *IEEE Int. Conf. on Network Infrastructure and Digital Content*, pp. 470–473, 2010.
- [6] Dries Neiryneck, Eric Luk, and Michael McLaughlin, “An alternative double-sided two-way ranging method,” *13th Workshop on Positioning, Navigation and Communication*, pp. 16–19, 2017.
- [7] Mohammed Ayman Shalaby, Charles Champagne Cossette, James Richard Forbes, and Jerome Le Ny, “Calibration and Uncertainty Characterization for Ultra-Wideband Two-Way-Ranging Measurements,” *arXiv: 2210.05888*, 2022.
- [8] IEEE Computer Society, *IEEE Standard for Low-Rate Wireless Networks. Amendment 1: Enhanced Ultra Wideband (UWB) Physical Layers (PHYs) and Associated Ranging Techniques (IEEE Std 802.15.4z)*, 2020.
- [9] Benjamin Hepp, Tobias Nægeli, and Otmar Hilliges, “Omni-directional person tracking on a flying robot using occlusion-robust ultra-wideband signals,” *IEEE Int. Conf. on Intelligent Robots and Systems*, pp. 189–194, 2016.
- [10] Taavi Laadung, Sander Ulp, Muhammad Mahtab Alam, and Yannick Le Moullec, “Novel Active-Passive Two-Way Ranging Protocols for UWB Positioning Systems,” *IEEE Sensors Journal*, vol. 22, no. 6, pp. 5223–5237, 2022.
- [11] Keith Vickery, “Acoustic positioning systems - a practical overview of current systems,” *IEEE Symposium on Autonomous Underwater Vehicle Technology*, pp. 5–17, 1998.
- [12] Sherman Lo, Yu Hsuan Chen, Per Enge, Robert Erikson, and Robert Lilley, “Distance measuring equipment accuracy performance today and for future alternative position navigation and timing (APNT),” *Int. Tech. Meeting of the Satellite Division of the Institute of Navigation, ION GNSS*, vol. 1, pp. 711–721, 2013.
- [13] Bhola Raj Panta, Kohta Kido, Satoshi Yasuda, Yuko Hanado, Seiji Kawamura, Hiroshi Hanado, Kenichi Takizawa, Masugi Inoue, and Nobuyasu Shiga, “Distance variation monitoring with wireless two-way interferometry (Wi-WI),” *Sensors and Materials*, vol. 31, no. 7, pp. 2313–2321, 2019.
- [14] Juri Sidorenko, Volker Schatz, Norbert Scherer-Negenborn, Michael Arens, and Urs Hugentobler, “DecaWave Ultra-Wideband Warm-Up Error Correction,” *IEEE Trans. on Aerospace and Electronic Systems*, vol. 57, no. 1, pp. 751–760, 2021.
- [15] Damien B. Jourdan, Davide Dardari, and Moe Z. Win, “Position error bound for UWB localization in dense cluttered environments,” *IEEE Trans. on Aerospace and Electronic Systems*, vol. 44, no. 2, pp. 613–628, 2008.
- [16] Václav Navrátil and František Vejražka, “Bias and variance of asymmetric double-sided two-way ranging,” *Navigation, Journal of the Institute of Navigation*, vol. 66, no. 3, pp. 593–602, 2019.
- [17] Ismail Guvenc, Sinan Gezici, and Zafer Sahinoglu, “Ultra-wideband range estimation: Theoretical limits and practical algorithms,” 10 2008, vol. 3, pp. 93 – 96.
- [18] Cung Lian Sang, Michael Adams, Timm Hörmann, Marc Hesse, Mario Pörrmann, and Ulrich Rückert, “Numerical and experimental evaluation of error estimation for two-way ranging methods,” *Sensors*, vol. 19, no. 3, 2019.
- [19] Qorvo, “Dw1000,” <https://www.qorvo.com/products/p/DW1000>.
- [20] Steven Kay, *Fundamentals of Statistical Signal Processing, Volume I: Estimation Theory*, Prentice Hall PTR, 1993.